Metadata of the chapter that will be visualized online

Series Title		
Chapter Title	Shape-Based Detection of Cortex Variability for More Accurate Discrimination Between Autistic and Normal Brains	
Chapter SubTitle		
Copyright Year	2011	
Copyright Holder	Springer Science + Business Media, LLC	
Corresponding Author	Family Name	El-Baz
	Particle	
	Given Name	**Ayman**
	Suffix	
	Division	Department of Bioengineering, Bioimaging Laboratory
	Organization	University of Louisville
	Address	304 Lutz Building, 40292, Louisville, KY, USA
	Email	aselba01@louisville.edu
Author	Family Name	Nitzken
	Particle	
	Given Name	**Matthew**
	Suffix	
	Division	Department of Bioengineering, Bioimaging Laboratory
	Organization	University of Louisville
	Address	304 Lutz Building, 40292, Louisville, KY, USA
	Email	
Author	Family Name	Casanova
	Particle	
	Given Name	**Manuel F.**
	Suffix	
	Division	Department of Bioengineering, Bioimaging Laboratory
	Organization	University of Louisville
	Address	304 Lutz Building, 40292, Louisville, KY, USA
	Email	
Author	Family Name	Khalifa
	Particle	
	Given Name	**Fahmi**
	Suffix	
	Division	Department of Bioengineering, Bioimaging Laboratory
	Organization	University of Louisville
	Address	304 Lutz Building, 40292, Louisville, KY, USA
	Email	
Author	Family Name	Sokhadze
	Particle	

Given Name	**Guela**
Suffix	
Division	Department of Bioengineering, Bioimaging Laboratory
Organization	University of Louisville
Address	304 Lutz Building, 40292, Louisville, KY, USA
Email	

Abstract

Autism is a complex developmental disability that typically appears during the first 3 years of life, and is the result of a neurological disorder that affects the normal functioning of the brain, impacting development in the areas of social interaction and communication skills. Early detection allows for treatments to be attempted, thus minimizing the impact of the autism on the individual. Given currently available diagnostic instruments, autism and other pervasive developmental disorders are difficult to detect in very young children. While shape based statistical analysis methods for autism are still in their early stages, current results show positive outlooks on the ability to detect differences between autistic and non-autistic patients. A framework is proposed that is capable of taking two-dimensional images from a standard medical scanner, and be able to construct a three-dimensional representation of the object and examine it through combination of its weighted linear spherical harmonics. The desired outcome is that a distinction can be made between the analysis of autistic and non-autistic brain data. The reconstruction analysis process involves linearly combining spherical harmonics of the corresponding mesh. It was expected that due to the complexity of the brain of an autistic subject it would require more iterations of reconstruction to reach convergence of the same error level as compared to the brain of a non-autistic subject. This was confirmed by the data. Using this method of analyzing the data a significant difference can be demonstrated between groups of examined subjects. The research clearly demonstrates that the non-autistic subjects' data converges both faster and with a lower rate of error level than the data taken from a person with autism.

Chapter 7
Shape-Based Detection of Cortex Variability for More Accurate Discrimination Between Autistic and Normal Brains

Matthew Nitzken, Ayman El-Baz, Manuel F. Casanova, Fahmi Khalifa, and Guela Sokhadze

Abstract Autism is a complex developmental disability that typically appears during the first 3 years of life, and is the result of a neurological disorder that affects the normal functioning of the brain, impacting development in the areas of social interaction and communication skills. Early detection allows for treatments to be attempted, thus minimizing the impact of the autism on the individual. Given currently available diagnostic instruments, autism and other pervasive developmental disorders are difficult to detect in very young children. While shape based statistical analysis methods for autism are still in their early stages, current results show positive outlooks on the ability to detect differences between autistic and non-autistic patients. A framework is proposed that is capable of taking two-dimensional images from a standard medical scanner, and be able to construct a three-dimensional representation of the object and examine it through combination of its weighted linear spherical harmonics. The desired outcome is that a distinction can be made between the analysis of autistic and non-autistic brain data. The reconstruction analysis process involves linearly combining spherical harmonics of the corresponding mesh. It was expected that due to the complexity of the brain of an autistic subject it would require more iterations of reconstruction to reach convergence of the same error level as compared to the brain of a non-autistic subject. This was confirmed by the data. Using this method of analyzing the data a significant difference can be demonstrated between groups of examined subjects. The research clearly demonstrates that the non-autistic subjects' data converges both faster and with a lower rate of error level than the data taken from a person with autism.

A. El-Baz (✉)
Department of Bioengineering, Bioimaging Laboratory, University of Louisville, 304 Lutz Building, Louisville, KY 40292, USA
e-mail: aselba01@louisville.edu

A. El-Baz et al. (eds.), *Multi Modality State-of-the-Art Medical Image Segmentation and Registration Methodologies*, DOI 10.1007/978-1-4419-8204-9_7,

7.1 Introduction

Autism is a complex developmental disability that typically appears during the first 3 years of life, and is the result of a neurological disorder that affects the normal functioning of the brain, impacting development in the areas of social interaction and communication skills. Difficulties can be identified in both children and adults with autism. The symptoms are identifiable in verbal and nonverbal communication, social interactions, and leisure or play activities. The classic form of autism involves a triad of impairments, these are typically in social interaction, in communication and the use of language, and in limited imagination as reflected in restricted, repetitive, and stereotyped patterns of behavior and activities [1].

The reported incidence of autism spectrum disorders has increased markedly over the past decade [2]. It is believed that autism affects the information processing found in the brain through the alteration of nerve collections and their synapses [3]. From Congress to popular media, speculation is increasing that more children have autism than ever before. The three classifications of autism include autism spectrum disorders (ASD), Asperger syndrome (AS) and pervasive developmental disorder (PDD) [4].

A study done in 2008 by Rapin and Tuchman [5], shows that autism is now recognized in 1 out of 150 children making it a prevalent disorder [5, 6]. Additional studies by DiGuiseppi show a high prevalence among screened American children with as high as 6.4% of screened children showing at least a mild form of an autistic spectrum disorder [7, 8]. According to the Centers for Disease Control and Prevention (CDC) in 2009, about 1 in 110 American children will fall somewhere in the autistic spectrum. Although the cause of autism is still largely not clear, researchers have suggested that genetic, developmental, and environmental factors may be the cause or the predisposing effects towards developing autism [9].

There are other mathematical relationships between incidence and prevalence. An important nuance about prevalence is that its accuracy is only as good as the degree to which each individual who actually has the condition is counted (the numerator or top number of the fraction), and the completeness with which the "general" or other population has been counted (the denominator or bottom number of the fraction.) Accuracy in these two figures can be hard to achieve. In fact, there are no scientifically based epidemiological prevalence estimates for ASD in the USA at this time. Federal agencies have, however, called upon researchers to submit proposals that will develop better prevalence rates [4].

Until research in the USA results in more accurate figures, the National Institutes of Health (NIH) have suggested the following prevalence rates for ASD based upon research in other Westernized, developing nations:

- 10/10,000 people with "classic" autism
- 20/10,000 people with ASD, including PDD
- 50/10,000 people with ASD, including PDD and Asperger syndrome

These estimates are inclusive; that is, the third estimate includes people in the first two groups. This means that in a given large population, on average 0.5%, one-half percent of the population could be diagnosed with an ASD [4].

Early detection allows for treatments to be attempted, thus minimizing the impact of the autism on the individual. Given currently available diagnostic instruments, autism and other PDD are difficult to detect in very young children. This may be due to several factors: presentation of symptoms varies from case to case; social and language deficits and delays may not be identified until the child is given the opportunity for peer interaction in preschool, low incidence leads to a low index of suspicion, and motor milestones are usually unaffected. Furthermore, there is no standard and easily administered screening instrument for young children. For all of these reasons, pediatric evaluations rarely identify autism before the age of three. However, evidence indicates that there is a large gap between the age of the child at the parents' first concern, the age of the first evaluation, and the age of a definitive diagnosis [8]. Parents are typically first concerned between the ages of 15 and 22 months (earlier for children who have co-morbid mental retardation), but the child is often not seen by a specialist until 20–27 months [14]. In addition, there is often further delay between the first visit to a specialist and a definitive diagnosis. However, evidence shows that this delay in diagnosis causes additional distress to parents, as well as wasting valuable intervention time, indicating that professionals in the field of autism need instruments to aid in the detection of autism in very young children [10].

Some forms of autism merely result in the individual exhibiting low social interaction, but more severe forms can result in severe mental retardation. These individuals may be prone to self-injuring and aggressive behavior. There is no current cure for any forms, of autism. However, educational, behavioral, or skill-oriented therapies were designed to remedy specific symptoms in each individual. Such therapies can result in a notable improvement for the individual, especially when begun at a young age [10].

7.1.1 Neuropathology of Autism

In identification of autism, the analysis of the neuropathology is important. The role of single-stranded microdeletions and epigenetic influences on brain development has dramatically altered our understanding of the etiology of the autisms. Recent research has focused on the role of synapse structure and function as central to the development of autism and suggests possible targets of interventions. Brain under connectivity has been a focus in recent imaging studies, and has become a central theme in conceptualizing autism. Despite increased awareness of autism, there is no "epidemic" and no one cause for autism. Data from the sibling studies are identifying early markers of autism and defining the broader autism phenotype [5].

The three sections of the brain analyzed are the gray matter, the white matter, and the corpus callosum. Examination of the individual sections shows significant

changes to the neuropathology of autistic individuals, suggesting a higher complexity in the autistic brain than the normal brain [11].

The gray matter is the brain cortex that contains the nerve cells responsible for routing sensory or motor stimuli to interneurons of the central nervous system. In autistic individuals Abel et al. [12] identified a decreased gray matter volume relative to a control group in the right paracingulate sulcus, the left inferior frontal gyrus, and an increased gray matter volume in amygdala and periamygdaloid cortex, middle temporal gyrus, inferior temporal gyrus, and in regions of the cerebellum. Additionally Boddaert et al. [13] found significant decreases of gray matter concentration in the superior temporal sulcus when comparing autistic child patients to normal child patients. The autistic children also demonstrated a decrease in white matter concentration located in the right temporal pole and in the cerebellum. Herbert et al. [14] applied a voxel-based-morphometry (VBM) approach to male patients between the ages of 7 and 11 years and showed that those with autism had a significantly larger volume of cerebral white matter (CWM) while cerebral cortex and hippocampus–amygdala had smaller volumes. The corpus callosum is largest single fiber bundle in the brain and is responsible for connecting the two hemispheres of the brain. It has been proposed that there are significant differences between the CC of autistic and normal patients [15, 16].

The concept that the cerebellum might play a role in the coordination of attention in a fashion analogous to the role it plays in motor control and that in autism, cerebellum mal-development is a consistent feature that renders the child unable to adjust his or her mental focus of attention to follow the rapidly changing verbal, gestural, postural, tactile, and facial cues that signal changes in a stream of social information [17]. Such cues signal the normal child to move his or her "spotlight of attention" from one source of information (e.g., auditory) to another (e.g., visual). This process involves disengaging attention from one source and then moving and reengaging it on another (i.e., inhibition of one source and enhancement of another). To selectively adjust the focus of attention, the nervous system must quickly and accurately alter the pattern of neural responsiveness to sensory signals – from an enhanced neural response to certain stimuli (e.g., vocalizations) to an enhanced response to other stimuli (e.g., gestures), and from inhibited neural response to some stimuli to inhibited response to others [18, 19].

7.1.2 Related Work

One method of early detection intervention, utilizes medical providers to screen children using the Modified Checklist for Autism in Toddlers (M-CHAT) as they were referred for early intervention services. The M-CHAT is designed to screen for early identification of autism spectrum disorder (ASD) in toddlers over the age of 12 months. Ideally, it is given at the 18–24 month well baby check. Parents complete the items on the checklist independently or by interview. Meeting the criteria suggests the risk of ASD and indicates a positive diagnosis for autism. The

purpose is to survey parents to determine how their child responds to varied stimuli from toddler locomotion to a child's reaction to other people. M-CHAT users also incorporate the M-CHAT Follow-up Interview into the screening process, given that recent findings demonstrate that the interview greatly reduces the false positive rate, which avoids unnecessary referrals [14]. Therefore, these children were considered to be at risk for a developmental disorder, but none had received any specific diagnoses and none had received more than several weeks of minimal intervention services.

In new experiments at Yale University, the researchers studied a group of 2-year-olds with autism, as well as typically developing children with developmental disabilities other than autism. The Yale program of research focuses on mechanisms of socialization and their disruption in the autism spectrum disorders. This work includes a close collaboration with Warren Jones in the development of novel techniques to quantify social processes using eye-tracking technologies with a view to visualize and measure the ontogeny of social engagement. New data analysis strategies have been used with children, adolescents, and adults with autism spectrum disorders revealing abnormalities of visual scanning behaviors when viewing naturalistic social approaches and situations. In this study autistic children showed a preference for audiovisual synchronicity in the use of "pat-a-cake" videos, while the other children were more interested in the figure's movements regardless of audiovisual synchronicity. That pattern could be a clue about brain development and early signs of autism [20–23].

Dr. Klin of Yale University explains that within a few days after birth, normal developing children prefer watching biological motion, the movement of living beings, such as their parents, and that preference is an important survival skill and a building block for relationships [21]. But Klin's group found that autistic children were more interested in "non-social contingencies," which are synchronicities that do not have any social meaning, like two balls colliding and making a sound, or a stone falling when someone drops it [20].

Researchers hope that a simple brain scan performed in infants and toddlers can presage the development of autism, leading to early detection and early intervention. The test involved using functional magnetic resonance imaging (MRI) to measure brain responses to spoken words in sleeping children. For this study, Dr. Eyler and her colleagues monitored the brain activity of 30 children with an autism spectrum disorder (aged 14 months to 46 months) and 14 "typical" children of roughly the same age [24].

Children slept in the MRI machine while researchers read them bedtime stories. This allowed the investigators to see which parts of the brain were being activated in typical children vs. children with autism. "In the typically developing children, both sides of the brain involved in language processing were activated. In the youngest children, the activation was about equal in both the right and left hemisphere, while in the older children, activity became more pronounced on the left side, which is similar to adult patterns and to be expected," Dr. Lisa T. Eyler explained. But in the autistic children, there was slightly more right hemisphere response than left hemisphere, and there was no change in activity across the age range [24].

David G. Amaral stated that "this leads to the conclusion that, in many children with autism, there are alterations either in structure growth or connectivity of the brain, but we really don't understand the implications of that for core features of autism, one of which is the problem with communication. This provides more evidence for abnormal connectivity in the brain." [24].

Further analysis of neurological MRI scans has been pursued in automated computer analysis of specific components of the brain. Approaches by El-Baz et al. [11] examine the shape model comparison between the corpus callosum in individuals with and without autism. This analysis focuses on comparison of the three-dimensional voxel positioning. In such an automated technique, specific areas of MRI scan images are extracted. These images are then placed in a stack to recreate a volume of the image. The difference between regions of this volume can be statistically measured. While statistical analysis methods are still in their early stages, current results show positive outlooks on the ability to detect differences between autistic and normal patients based on voxel-based analysis. The positive findings from automated analysis research provide the basis for the research done in this chapter.

There are many different methods that can be used to examine objects for difference. In the area of autism detection and analysis, Gyral Window Index (GWI) and volumetric descriptions of brain structures (volume analysis) are the most common ones.

GWI analysis involves counting the gyrations found along the brain in various areas and comparing these counts to make an assumption. This technique is heavily prone to error in that brains that drastically differ in shape and complexity may show little to no difference and brains of similar shape and complexity could show a large difference.

Volumetric descriptions of brain structures examine the volume of an object. This is also commonly known as volume analysis. In this the volumes of objects are compared. While this does relay important information, it is not optimal for examining a complex organ. Imagine that you have two bowls. One of these is shaped like a large flat saucer and the other is shaped like a very thin vase. Assume that both of these will hold the same amount of liquid when filled. This example illustrates the flaws of volume based analysis on an object. While the volumes are identical for the two objects, the shape and complexity is drastically different. An example of this type of phenomenon can be seen in Fig. 7.1 illustrated by a clear plastic geometry set.

Shape analysis is an alternative method to the previous two. In these the shape is represented by a complex mesh of nodes. These nodes fall within respective areas on the surface and can be compared to one another to determine differences. Instead of examining the volume or visual changes along the cortex of the brain the locations of points on the brain are examined and compared based on their locations in space. This examination performs a comparison between specific points as illustrated in Fig. 7.2. It is important to maintain strict rules on construction and examinations of objects when using this technique to ensure accuracy. This chapter will focus on a framework for the analysis of the cortex using shape analysis through the construction and examination of spherical harmonics.

Fig. 7.1 Containers that all hold an identical volume with dramatically different shapes

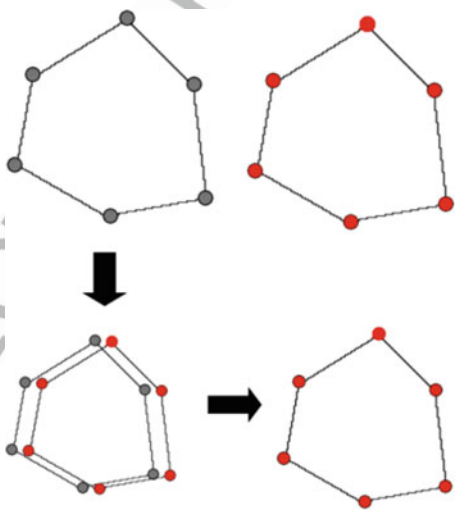

Fig. 7.2 Illustrating the comparison between points representing an object in shape analysis instead of examining the object as one volumetric entity

7.2 Methods

The proposed analysis system is subdivided into the parts found in Fig. 7.3. This section will primarily cover the second and third rows in the flowchart which pertain to three-dimensional mesh construction and to the analysis of a mesh using spherical harmonics. The initial data consists of segmented MRI images of data.

First, the raw recorded image data is passed through a system to remove the skull from the image. This is done using the software called MRIcro developed by Chris Rorden from the Neuropsychology Lab and Georgia Institute of Technology in Altlanta, GA [25–28]. This software examines the raw image and removes and pixel data pertaining to the skull leaving only brain matter remaining as shown in

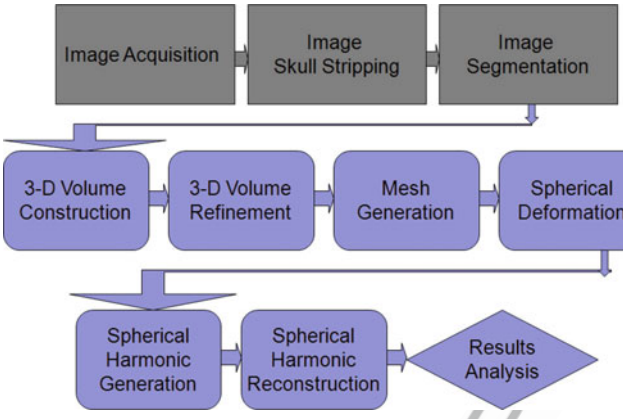

Fig. 7.3 Flowchart of the proposed analysis system

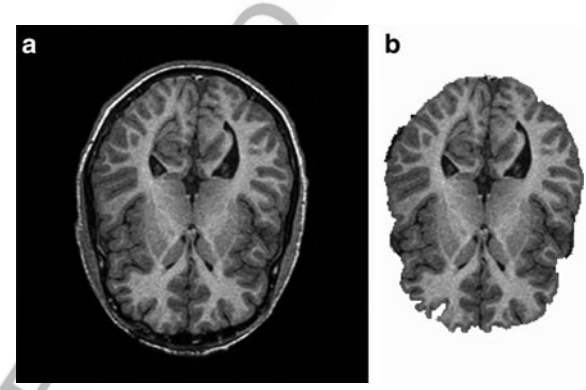

Fig. 7.4 (**a**) Typical MRI image, (b) image after removal of skull from around the brain using MRIcro

Fig. 7.4. After this the image is segmented to a binary representation. The image is inverted so that the brain received by the framework has a black background and the brain data is the white area.

For each image, a black pixel represented the background or portions of the image where no data existed, and the white pixels represented areas where data existed (Fig. 7.5). Often images formats do not store data in binary form and data is stored using a variation of a grayscale format. The individual pixel values range from 0 to the maximum grayscale value (in many cases this value was 255 and represented a white pixel.) It can be assumed then that any pixel with a value greater than zero would constitute a pixel containing data. Setting all pixels to the desired limits can be accomplished by dividing the matrix by the maximum value and then taking using a ceiling command on the data.

After each image is converted to a binary representation, the images are assembled in a three-dimensional matrix stack. Each matrix is represented by an X, Y, and Z dimension. The X dimensions represent the rows in an image, the Y dimension represents the columns in an image, and the Z dimension represented the layers in

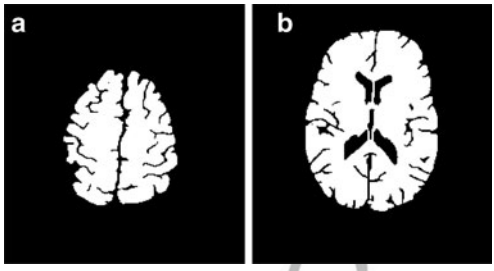

Fig. 7.5 Examples of segmented brain data used as input data

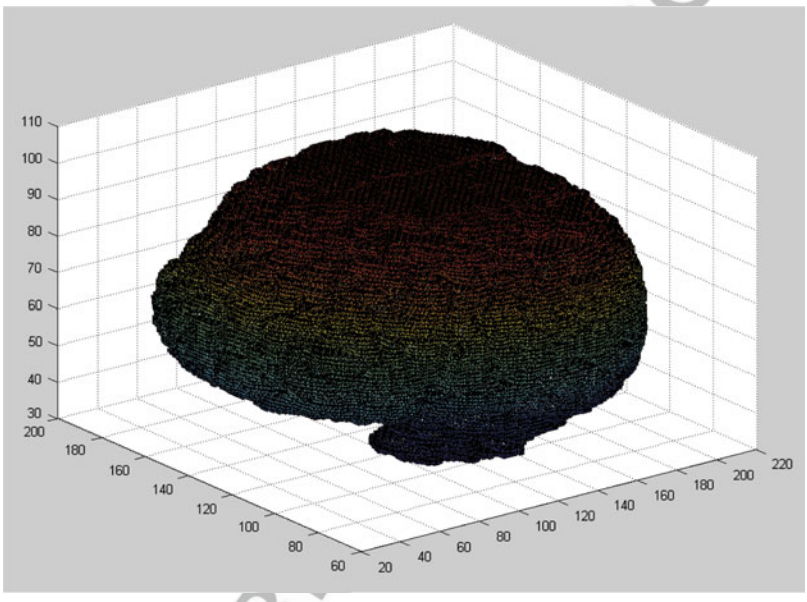

Fig. 7.6 Three-dimensional binary representation of a brain

the volume, with each layer encompassing a separate distinct image. Each coordinate (x, y, z) represented a single voxel in three-dimensional space and the combination of the voxels is a rough three-dimensional representation of the object to be analyzed. Figure 7.6 illustrates a generic representation of a three-dimensional volume as viewed using Matlab.

In this framework the images are loaded into the memory without preprocessing to remove holes in the images. This is done because when the images are compiled into a shape in three-dimensional space, holes can be created by the placement of layers on top one another. It is a simpler process to simply execute an algorithm to remove these holes using one processing step than to perform both pre and post processing on the volume. While initially the decision was made to remove all holes in the two-dimensional images prior to being loaded into the program, this proved ineffective after the images were placed in a three-dimensional volume. To remove these holes from the image, a hole detection algorithm can be used.

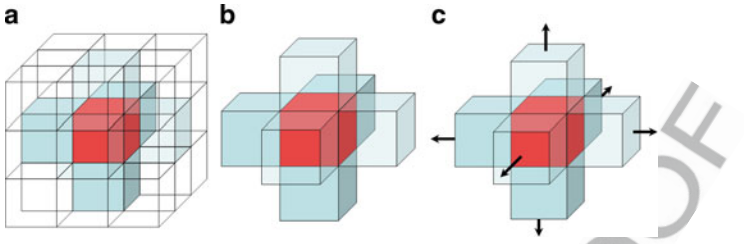

Fig. 7.7 (**a**) The original cube of pixels, (**b**) showing the starting neighbor pixels in the six cardinal directions, (**c**) the outward directions of movement for the detection iterations

The algorithm begins by loading the images into the three-dimensional volume matrix as previously described. After creating the three-dimensional volume matrix, an iterative pass is made across the X, Y, and Z axis of the volume using the Matlab "fillholes" command. To accomplish this, a two-dimensional image slice is removed on each plane of the volume. This image slice was then passed through the "fillholes" algorithm, and the modified image slice was reinserted into the volume. In this way, the holes were removed from the two-dimensional representations in the X, Y, and Z directions.

Following this procedure, additional small holes not removed using the previous method are scanned for and removed. To remove these additional holes, each individual pixel is iterated in the three-dimensional matrix. For each pixel, it is calculated if there was a pixel belonging to the image in the $\pm X$, $\pm Y$, and $\pm Z$ directions between the origin pixel and the edge of the volume. In Fig. 7.7a, the origin pixel is defined as the red pixel, the blue neighbor pixels are the $\pm X$, $\pm Y$, and $\pm Z$ directional pixels, and the clear pixels represent unchecked points. Figure 7.7b shows the same image with the unchecked pixels removed for easier visibility. From the image points, outgoing vectors were tested in each of the six directions. Figure 7.7c illustrates the path of testing that each neighbor pixel would expand from towards the outer edge. If a pixel value of 1 is found in a given direction, a value of true is marked for the boolean corresponding with that direction.

If a pixel is found radiating out in all six directions, it is determined that the pixel was a hole in the image. A pixel that does not contain pixels surrounding it on all six sides is ignored. This procedure is repeated until holes are removed from the image. This is often accomplished in a single iteration. To ensure that the volume is clean, an additional iteration is repeated that verifies that no holes remain in the volume.

7.2.1 Mesh Generation

Once the three-dimensional volume has been properly constructed, the mesh can be generated. In this framework, the mesh generation is performed using a modified version of the iso2mesh Matlab based mesh generation system, written by Qianqian

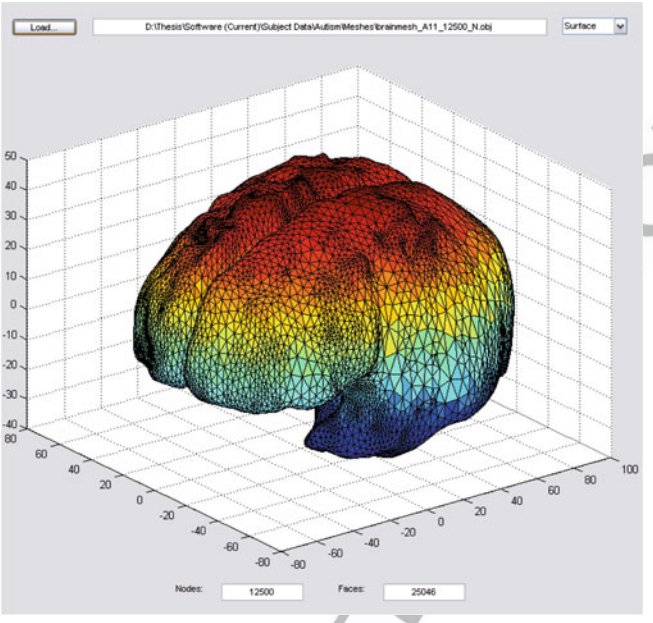

Fig. 7.8 Mesh render for the cortex of an autistic person

Fang and David Boas [29, 30]. A sample mesh render is illustrated in Fig. 7.8. This system is built on the CGAL Delaunay Triangulation mesh engine. This is a nonrigid mesh generation engine, and points are not constrained to contain a specific number of neighboring nodes. The modifications to the original iso2mesh code are to enable restriction of node counts and to generate a raw nonprocessed mesh. The restriction of node counts is important to ensure that objects being compared have the same properties. The raw mesh is recovered from the iso2mesh package before any of the post processing and surface analysis is performed on it. For this framework, these alterations are not necessary and can lead to complexity problems in the mesh.

The data received from the mesh generation is a collection of nodes and triangulations. The nodes matrix is of dimensions $3 \times N$, and the triangulations matrix is of dimensions $4 \times T$, where N is the maximum allowable amount of nodes and T varies based on the positions used by the mesh engine and the triangulations created between points. The combination of three triangulation points connected with one another represents a face found on the corresponding mesh and each row in the triangulations matrix contains data representing a unique face. The fourth column in the triangulation matrix is a boolean value representing that the face connectivity at this point exists. Following mesh creation, all values in this fourth column will be equal to true and this column can thus be removed to create the traditional $3 \times T$ representation found in a mesh triangulation matrix.

Once the initial mesh is created, it is necessary to reposition it in three-dimensional space and to resize the mesh to appropriate proportions. The centroid

of the mesh is calculated in the X, Y, and Z directions. Using the coordinates of the centroid, the mesh is repositioned so that it is centered on the origin in three-dimensional Cartesian space ($x = 0$, $y = 0$, $z = 0$). Because of data acquisition limitation the original mesh is not scaled properly. It is necessary then to appropriately resize the mesh using the original image slice acquisition scaling. The mesh coordinates are then repositioned according to the X, Y, and Z magnification parameters of the scanner used to acquire the images. The X and Y planes are multiplied by a magnification factor of 0.93 in this example, taken from the MRI scanner acquisition parameters. The Z plane is scaled by a factor of 1.5 in this example, the distance between slices taken during MRI acquisition. The result is a properly scaled mesh that is centered around the origin in three-dimensional space.

The raw mesh generation returns a node and face cluster where vertex points contain a large amount of noise. ~~To remove this, noise a~~ vertex-based anisotropic smoothing filter is applied to the data. The filter performs a low-pass filter Laplacian smoothing algorithm across the exterior of the mesh. The low-pass filter Laplacian smoothing algorithm used in this framework is based on code written by Zhang and Hamza [31]. The smoothing algorithm is applied iteratively three times during the procedure, and is configured to smooth at a minimal value with each pass. The final mesh is accurately scaled and correctly positioned in three-dimensional space and contains smooth and accurate contours representing the various locations found on the cortex.

The file format chosen to save the mesh data in this framework is the Wavefront OBJ format, developed by Wavefront Technologies. The standardized Wavefront OBJ format is used because it is a common mesh file representations used in a majority of commercial and open-source application mesh analysis applications and will allow for potential future integration of the framework with third-party software. Custom algorithms have been written to write and save meshes in this format in a way that is universally compatible. The algorithms used follow all standard guidelines for the common Wavefront OBJ format.

7.2.2 *Spherical Deformation*

Following the generation of a stable, hole-free initial mesh, it was necessary to generate a corresponding unit sphere. The accuracy of the sphere creation is relative to the accuracy of the statistical analysis. There were several techniques attempted including Cartesian and spherical registration methods.

The initial attempt to create a unit sphere involved simply inflating the original mesh into a unit sphere. This technique was done by reducing all points in the mesh to a maximum distance of 1.0 from the origin. Once the mesh had been scaled, all points with a value less than 1.0 were up scaled to a value of 1.0. This inflation technique resulted in numerous problems, with the most problematic being vertex overlap and poor distribution of points. The natural shape of the brain sulci and the valley located between hemispheres in the brain created this overlap by inverting

points and face connectivity, as they were forced to the outer edges of the inflated sphere. This occurred due to the fact that multiple points existed along the same or incorrect θ and φ angles in spherical space.

In the creation of a unit sphere, it became imperative that all points remain in their correct orientation with their neighbor points during the deformation process. This means that during deformation, the triangulation connections could not become crossed. A unit sphere that contained crossed triangulations produced an erroneous spherical representation. This is because during calculation of the harmonics it assumes that the detected neighboring nodes are truly the neighbor nodes for a given vertex. If the points become misplaced or shifted to an erroneous location away from its true position than a neighboring node may appear to be falsely connected to additional nodes. The spherical harmonics are based on angular values, and points with incorrectly crossed angles caused the system to produce poor resultant data making a spherical reconstruction not possible.

The accuracy of the spherical representation was also based on the distribution of the vertex coordinates throughout the sphere and the accuracy to it being a true unit sphere. A sphere with clusters of vertices and other areas of sparse vertex placement produced significantly more error and had a greater difficulty converging. The ideal spherical representation will have all vertices spaced equidistant from one another across the surface of the sphere. While it is possible to perform an analysis using an improperly spaced unit sphere, the results were less than desirable. The original method leaves large clusters of vertices around areas of significant sulcus curvature in the brain.

The process, used in the creation of a unit sphere is a multiple phase deformation technique, created for the purpose of deforming the brain meshes. Before running the spherical deformation, the brain was heavily smoothed using a Laplacian based smoothing algorithm. The mesh was loaded into the freely available software, MeshLab v1.2.3b written by Paolo Cignoli [32, 33]. It was determined through trial and error that an average smoothing of 400 iterations per 12,500 nodes deformed the mesh so that no existing points in the mesh could be found residing on the same θ and azimuth angles, when examined in spherical coordinate space (Fig. 7.9). MeshLab was used to improve processing speed during the smoothing phase. The comparable Matlab algorithm took approximately 30 seconds to run one

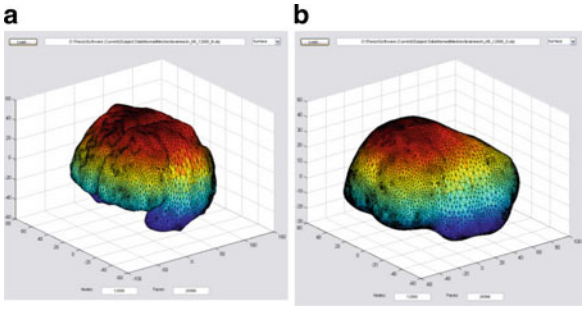

Fig. 7.9 (**a**) An original brain render and (**b**) the render after 400 iterations of Laplacian smoothing

complete Laplacian smoothing pass. The same algorithm run in MeshLab was capable of performing 2000 Laplacian smoothing passes in slightly under one minute.

Algorithm 1: Spherical Deformation Algorithm

1. *Deformation of original mesh into smoothed mesh model.*
2. *Expansion of smoothed mesh model distances to distance of unity sphere.*
3. *Application of attraction–repulsion algorithm for node positioning refinement on expanded mesh.*
4. *Expansion of refined mesh model distances to distance of unity sphere.*

The Spherical Deformation Algorithm was used to transform the shape of a constructed mesh to that of a unity sphere. In the Laplacian deformation phase, the brain is smoothed until all curves, peaks, and valleys of the cortex are flattened across the brain. This ensures that no more than one point will be found for a given set (azimuth and θ angles) of spherical coordinates. This mesh is then resaved as a smooth mesh object which will be loaded for the second through fourth phases.

The unit sphere distance deformation involves inflating the smoothed mesh to the distance of a unit sphere. To increase the speed of the spherical inflation it is necessary to manipulate the mesh in the spherical coordinate domain. The Cartesian mesh is first converted to spherical coordinates using the *cart2sph* command in Matlab. This returns a θ angle, azimuth (φ) angle, and R distance for each point in the mesh. The R distance is removed and replaced with a matrix of the same size with all values equal to 1.0. The coordinates are then reconverted to Cartesian using the *sph2cart* command in Matlab. This provides a fast and effective conversion that is extremely efficient, because it requires no iterative processing and does not involve examining each node individually or performing any distance calculations. These inflated points are then passed on to the third phase.

In the third phase, the attraction–repulsion algorithm is used to refine the inflated sphere. The attraction–repulsion algorithm is based on a standard spring algorithm. The algorithm was inspired by a concept used in Graphic Art Design for inflating objects. The purpose of this algorithm is to reposition the nodes in the mesh. After the second phase of the spherical deformation, there are large clusters of nodes spaced near one another in areas of the mesh that contain a high density of nodes. Looking at the mesh, it is possible to see large clusters near the lower lobes of the brain and around complex areas. As previously mentioned, it is necessary to evenly space the nodes across the sphere. To accomplish this, the attraction–repulsion algorithm was created.

The attraction–repulsion algorithm is composed of two steps, the attraction step and the repulsion step. Each node is altered by being processed in the attraction step and then the repulsion step. In the attraction step, the node is altered based on its neighbor nodes. The distance between a node and each of its neighbor nodes is calculated. The node is then pulled based on numerical weighting, so that it becomes centered between its neighbors. The attraction for iteration i is defined as:

$$A_{i+1} = A_i + (\overline{Q_N P_J})(D^2)(0.01) + (\overline{P_J Q_N})\left(\frac{0.00001}{D}\right), \quad (7.1)$$
$$1 \le j \le \text{number of nodes}, \quad 1 \le N \le \text{number of neighbors}$$

where A_{i+1} represents the new node coordinate and A_i is the original node coordinate. P represents the original coordinate of the unmodified node that is and Q is the coordinate of neighbor node N. The distance (D) from P to Q is a three-dimensional Euclidean distance.

After the node has been centered between its neighbors it is processed in the repulsion step. Here the node is slightly readjusted by every node in the mesh. Each node minimally repels one another so that the nodes do not cross or touch. The repulsion is defined as:

$$R_{i+1} = R_i + (\overline{Q_k P_J})(T)\left(\left(\frac{1.5}{(\overline{Q_k P_J})^2}\right)\left(\frac{1}{2N}\right)\right), \quad (7.2)$$
$$1 \le j \le \text{number of nodes}, \quad 1 \le k \le \text{number of nodes}$$

where $R_i + 1$ represents the new node coordinate and R_i is the original node coordinate. N represents the total number of nodes in the mesh. T is a value between 0 and 1 and stands for the time step of the algorithm. A larger time step enables the algorithm to converge faster, but increases the chance of error as nodes are capable of moving larger distances.

This algorithm also causes an inflation effect to occur during repeat iterations as each node is gently repelled from interior angles by nodes opposite it on the unit sphere. Because there are no nodes outside the unit sphere to repel the nodes back toward the center this inflation occurs. This step is repeated several times until a satisfactory node distribution is reached (Figs. 7.10 and 7.11). Once the attraction–repulsion algorithm has completed, the nodes are more evenly spaced on the sphere. Due to the previously described interior repulsion, the sphere is also much larger than a unit sphere of radius 1 at this point. To alleviate this phenomenon, the unit sphere distance deformation algorithm is run a second time. While this algorithm does not alter the angular placement of the nodes, it will reduce the R values back to 1 for all nodes. This is the same algorithm that is run during phase two. Following this deformation, the newly created unit sphere mesh is written back into a Wavefront OBJ file.

7.2.3 Spherical Harmonic Analysis

The weighted spherical harmonic representation (weighted-SPHARM) is a surface modeling framework that can be used in encoding cortical shape information. The technique was developed by Moo K. Chung, Kim M. Dalton and Richard J. Davidson.

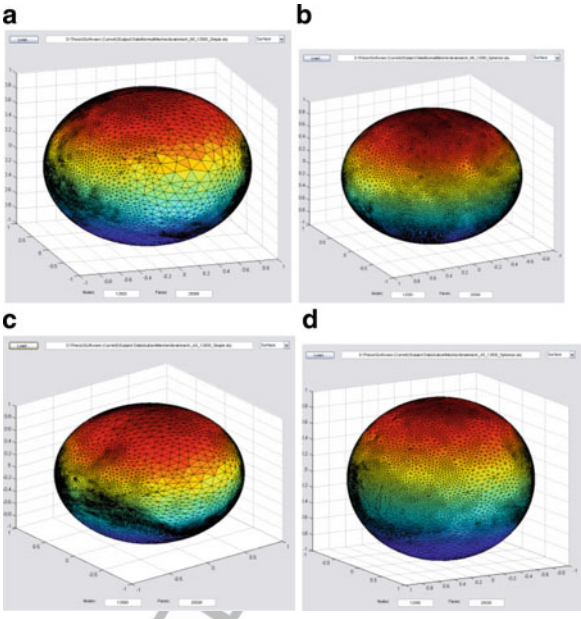

Fig. 7.10 (**a**, **c**) Simple spherical inflations of subject brains. (**b**, **d**) The respective corresponding unit spheres after three iterations of the attraction–repulsion algorithm have been applied

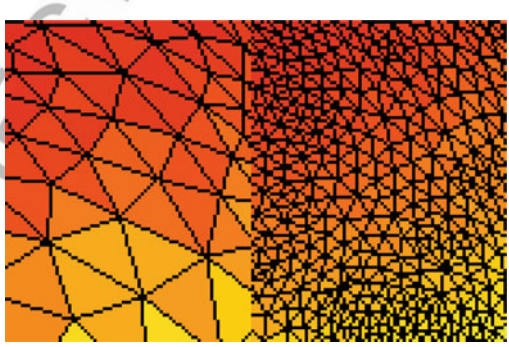

Fig. 7.11 Detailed view of the same region before and after application of the attraction–repulsion algorithm

The weighted-SPHARM representation is a spectral method [34], where a linear combination explicit basis functions is used to represent noisy cortical surface data. The basis expansion corresponds to the solution of an isotropic heat equation on a unit sphere. The result of the weighted-SPHARM is explicitly given as a weighted linear combination of spherical harmonics. This provides a more natural setting for statistical modeling. The representation can be further used in surface registration that reduces the improper alignment of brain sulcus folding patterns between subjects and across hemispheres within a subject.

The system generates harmonics from the original distribution of coordinates. This ensures that the same neighbor nodes are connected in the same order between the original and the reconstructed mesh. The harmonics are specifically generated

from the unique unit sphere corresponding to the original mesh. The original Cartesian coordinate system of the corresponding unit sphere mesh parameterizes a coordinate $v_i = v(x, y, z)$ to spherical coordinates with a polar angle between 0 and π and an azimuth angle between 0 and 2π. Each point is then represented as a spherical coordinate that can be expressed as $v_i = v(\theta, \varphi)$. The distance from the origin, or R value, in spherical space is always equal to 1.0 for any given point on a unit sphere [35]. The paper by Chung et al. defines the values of θ and φ for purposes of calculation as:

$$\theta_{\text{SPHARM}} = \frac{\pi}{2} - \varphi, \quad \varphi_{\text{SPHARM}} = \pi + \theta. \tag{7.3}$$

The spherical harmonic Y_{lm} of degree l and order m [36, 37] is defined as:

$$Y_{lm} = \begin{cases} c_{lm} P_l^{|m|}(\cos\theta)\sin(|m|\varphi), & -l \le m \le -1 \\ \frac{c_{lm}}{\sqrt{2}} P_l^{|m|}(\cos\theta), & m = 0 \\ c_{lm} P_l^{|m|}(\cos\theta)\cos(|m|\varphi), & 1 \le m \le l \end{cases}, \tag{7.4}$$

$$c_{lm} = \sqrt{\frac{2l+1}{2\pi}\frac{(l-|m|)!}{(l+|m|)!}}, \tag{7.5}$$

where $P_1^{|m|}$ is the associated Legendre polynomial of order m [35, 36]. These form a form a polynomial sequence of orthogonal polynomials [35].

For the purpose of this chapter only nonnegative harmonics were used. For each degree Y_{lm} represents the Fourier coefficients capable of reconstructing the spherical harmonic as specified in code written by Moo K. Chung. This code saves the coefficients of the spherical harmonic in a new file for each degree. These can then be reloaded to expedite future calculations [34].

A final reconstruction is created by iteratively using the desired number of harmonics to reconstruct the original brain in a linear fashion. As each harmonic is loaded into memory, it is multiplied by a factor sigma which is equivalent to the smoothing of the harmonic. A larger sigma value indicates a higher degree of smoothing, while a smaller sigma value preserves more of the data from the current harmonic degree. These values are then linearly added to the previous coordinate value, and the new coordinate is formed. During reconstruction of the original mesh, the surface coordinates can be modeled independently according to the equation:

$$v_i(\theta, \varphi) = h_i(\theta, \varphi) + \varepsilon_i(\theta, \varphi), \tag{7.6}$$

where $v_i(\theta, \varphi)$represents the new coordinate, $h_i(\theta, \varphi)$ represents the original coordinate, and $\varepsilon_i(\theta, \varphi)$ is the linear modifier constructed from the combination of the smoothing σ value and the residual Fourier values for the specified coordinate calculated for the current spherical harmonic degree. This procedure is repeated for

the desired number of harmonics, and a final resulting mesh is produced and returned to the user [37].

The error between the reconstructed brain mesh and the original brain mesh is found by calculating the three-dimensional Euclidean distance between corresponding points in the original mesh and the reconstructed mesh. Due to the strict ordering of the data storage in the harmonics, the reconstructed mesh and the original mesh are already registered to one another, and thus do not require additional registration, simplifying the calculations required. Additionally, for visualization purposes, the same connected set of faces is used for both the original and reconstructed mesh [37].

All subject data was processed identically, and results were analyzed for σ smoothing values of 0.01, 0.001, 0.0001, and 0.00001. There were 10 subjects in the autistic group and 12 subjects in the non-autistic group. The error for each reconstruction was calculated for every set of harmonics in each of the patients. These errors were then analyzed to find the iteration at which a reconstructed brain demonstrated accuracy below a certain threshold. The thresholds of 11 and 10% were selected for accuracy. Due to the slow convergence of many of the autistic brains, an iteration value of 61 has been used to represent that the brain did not converge below the threshold within the initial 60 iterations used.

As the smoothing due to Fourier reconstruction across the mesh is reduced, the amount of data used from each harmonic is increased. The harmonics begin to converge much faster in these reconstructions. The error curves for each data set show the rate of convergence and the maximum convergence visually for a specific brain. The convergence curves at the two extremes for smoothing can be seen in Fig. 7.12.

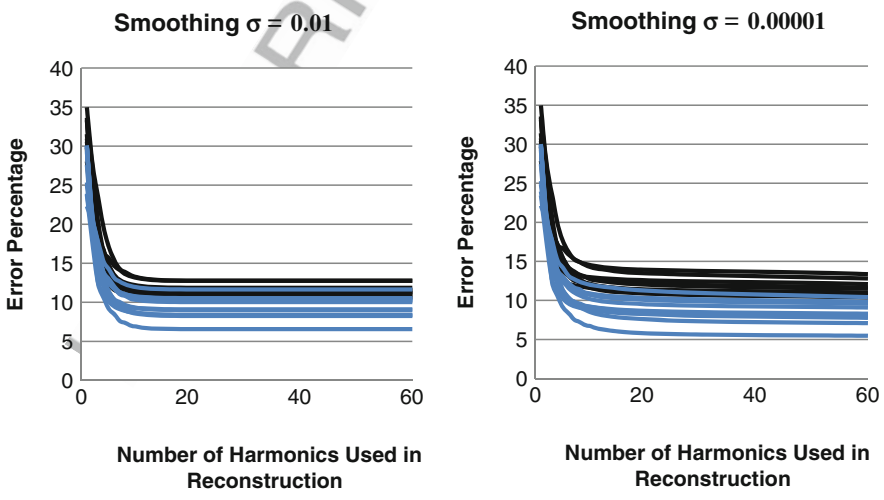

Fig. 7.12 Convergence curves for the two extreme values of sigma

11%Error 10%Error

Analysis using smoothing σ = **0.01**

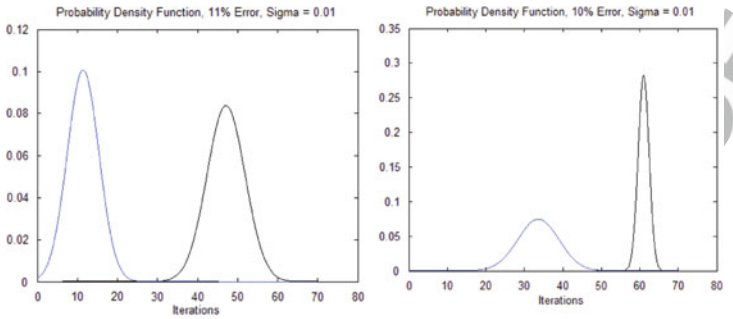

Analysis using smoothing σ = **0.001**

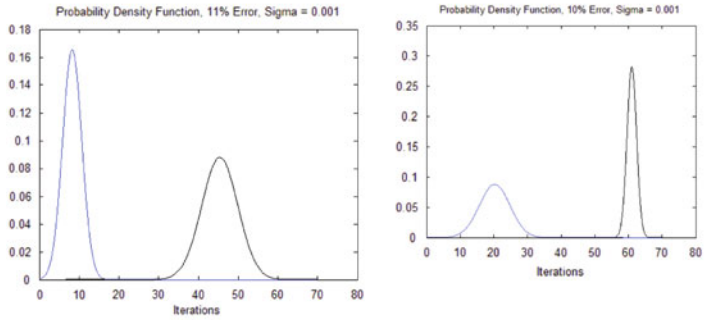

Analysis using smoothing σ = **0.0001**

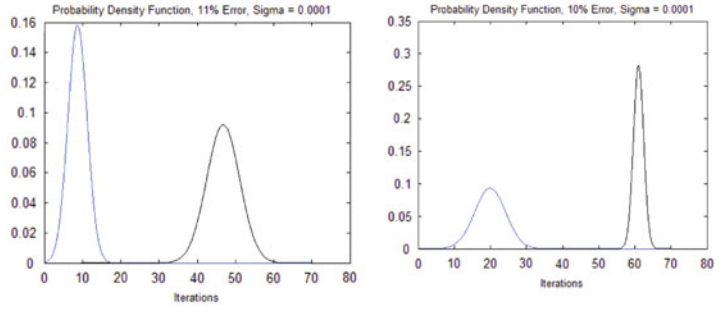

Analysis using smoothing σ = **0.00001**

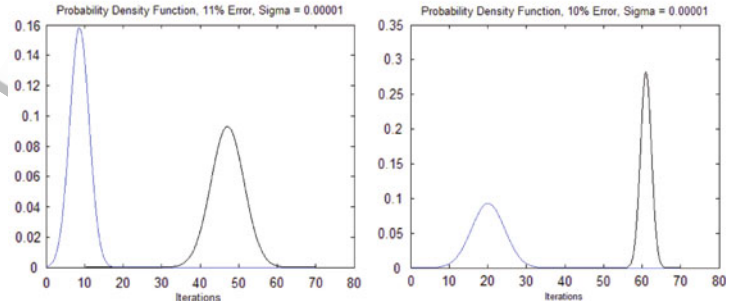

Fig. 7.13 Probability Density Function plots at decreasing levels of σ

It is important to note the overlap between the blue and black lines in the first image in the figure and the sharp distinction between the blue and black lines in the second image. The blue lines represent convergence of subjects not demonstrating autism while the black lines represent subjects who positively demonstrated autistic characteristics.

Probability density functions (pdf) were generated for each error threshold as well using the mean and standard deviation applied to a Gaussian fit pdf. This gives the likelihood of classification for a given number of iterations to convergence. The black lines (right peaks in all images) represent the data for the subjects demonstrating autism while the blue lines (left peaks in all images) represent subjects not demonstrating autism. This shows that the probability of a subject requiring a low number of reconstruction iterations to converge below a given threshold is likely to not be autistic.

7.3 Conclusion and Future Work

Considering the data from previous methods including Modified Checklist for Autism in Toddlers, eye-tracking technologies, and the prevalence of the disorder, it is essential to find alternate and scientific methods that include brain analysis as a diagnostic and evaluative method. The research of doctors at Yale has determined that brain scans can predict the development of autism, leading to early detection and early intervention.

Using this method of analyzing data can demonstrate accurate differences in normal and autistic brains. The research that has been generated in this chapter can clearly demonstrate that the normal brain data converged both faster and with a lower rate of error level than the Autistic brain data. This result proves that the autistic brain is a more complex structure, and would be more difficult to reconstruct using this shape-based detection of cortex variability process.

The flexibility of the created package is of additional importance to the expansion of the project. The algorithms and theories introduced in this chapter can readily be applied to any object freely. The object can be converted from two-dimensional scans into a three-dimensional mesh, deformed and analyzed. This would allow for future analysis of many other organs including cancerous growths and individual components of the brain. Examining the difference between reconstructions can enable change in an object to be tracked over time and compared as well. This would allow for an analysis of the rate of the progression of autism in the individual. This can provide valuable information that can be used to improve treatments by providing physicians with a detailed mathematical representation of the current state of their patient.

It is also plausible to use a technique similar to this one to understand what areas of the brain begin to alter at different times in the subject and to track their impact on the overall autism. Gaining a detailed understanding of the progression of autism in patients can help lead to meaningful solutions for autistic patients.

After numerous attempts to create a package for shape-based detection of cortex variability, the primary difficulties arose in generating an accurate mesh from a variety of data and deforming the mesh into an accurate unit sphere while preserving the integrity and positioning of nodes within the mesh. Through the combination of techniques from a variety of fields including engineering, computer science and graphical art design these challenges were overcome. Using this technique it will be possible to analyze a large variety of MRI scans to compare the complexities of normal and Autistic brains.

Future plans are to improve the efficiency of the algorithms to allow accurate deformation and analysis of larger and more detailed mesh structures. Improvements in the algorithm will allow for faster and more accurate analysis of the subject. As previously mentioned, it is also planned to make the package more flexible so that it can readily be applied to a variety of structures and used as a meaningful evaluation technique for multiple disorders.

References

1. Minshew NJ, Payton JB (1988) New perspectives in autism, part I: the clinical spectrum of autism. Curr Probl Pediatr 18(10):561–610
2. Schaefer GB, Mendelsohn NJ (2008) Clinical genetics evaluation in identifying the etiology of autism spectrum disorders. Genet Med 10(4):301–305
3. Losh M, Adolphs R, Poe MD, Couture S, Penn D, Baranek GT, Piven J (2009) Neuropsychological profile of autism and the broad autism phenotype. Arch Gen Psychiatry 66(5):518–526
4. Jacobson JW (2000). Is autism on the rise? Science in Autism, vol 2, no 1
5. Rapin I, Tuchman RF (2008) What is new in autism? Curr Opin Neurol 21(2):143–149
6. Department of Developmental Services (1999) Changes in the population of persons with autism and pervasive developmental disorders in California's developmental services system 1987 through 1998. Author, Sacramento, CA
7. Department of Education (1999) Digest of education statistics, 1998. Author, Washington, DC (GPO No. 065-000-01174-3, NCES No. NCES 1999036)
8. DiGuiseppi C, Hepburn S, Davis JM, Fidler DJ, Hartway S, Lee NR, Miller L, Ruttenber M, Robinson C (2010) Screening for autism spectrum disorders in children with Down syndrome: population prevalence and screening test characteristics. J Dev Behav Pediatr 31(3):181–191
9. Stevens M, Fein D, Dunn M, Allen D, Waterhouse LH, Feinstein C, Rapin I (2000) Subgroups of children with autism by cluster analysis: a longitudinal examination. J Am Acad Child Adolesc Psychiatry 39:346–352
10. Robins DL, Fein D, Barton M, Green J (2001) The modified checklist for autism in toddlers: an initial study investigating the early detection of autism and pervasive developmental disorders. J Autism Dev Disord 31(2):131–144
11. El-Baz A, Elnakib A, Casanova M, Gimel'farb G, Switala A, Jordan D, Rainey S (2010) Accurate automated detection of autism related corpus callosum abnormalities. J Med Syst. doi:10.1007/s10916-010-9510-3
12. Abell F, Krams M, Ashburner J, Passingham R, Friston K, Frackowiak R, Happe F, Frith C, Frith U (1999) The neuro-anatomy of autism: a voxel-based whole brain analysis of structural scans. Neuroreport 10(8):1647–1651
13. Boddaert N, Chabane N, Gervais H, Good CD, Bourgeois M, Plumet MH, Barthelemy C, Mouren MC, Artiges E, Samson Y, Brunelle F, Frackowiak RSJ, Zilbovicius M (2004)

Superior temporal sulcus anatomical abnormalities in childhood autism: a voxel-based morphometry MRI study. Neuroimage 23:364–369
14. Herbert MR, Ziegler DA, Deutsch CK, O'Brien LM, Lange N, Bakardjiev A, Hodgson J, Adrien KT, Steele S, Makris N, Kennedy D, Harris GJ, Caviness VS Jr (2003) Dissociations of cerebral cortex, subcortical and cerebral white matter volumes in autistic boys. Brain 126:1182–1192
15. Egaas B, Courchesne E, Saitoh O (1995) Reduced size of corpus 576 callosum in autism. Arch Neurol 52(8):794–801
16. Schumann CM, Barnes CC, Lord C, Courchesne E (2009) Amygdala enlargement in toddlers with autism related to severity of social and communication impairments. Biol Psychiatry 66(10):942–949
17. Courchesne E, Press GA, Yeung-Courchesne R (1993) Parietal lobe abnormalities detected with MR in patients with infantile autism. AJR Am J Roentgenol 160(2):387–93
18. Schumann CM, Bloss CS, Barnes CC, Wideman GM, Carper RA, Akshoomoff N, Pierce K, Hagler D, Schork N, Lord C, Courchesne E (2010) Longitudinal magnetic resonance imaging study of cortical development through early childhood in autism. J Neurosci 30 (12):4419–4427
19. Kennedy DP, Courchesne E (2008) Functional abnormalities of the default network during self- and other-reflection in autism. Soc Cogn Affect Neurosci 3(2):177–190
20. Hitti M, Chang L (2009) Autism: new clue to earlier detection. WebMD Health News. March 29, 2009
21. Klin A, Lin DJ, Gorrindo P, Ramsay G, Jones W (2009) Two-year-olds with autism orient to non-social contingencies rather than biological motion. Nature 459(7244):257–261
22. Jones W, Klin A (2009) Heterogeneity and homogeneity across the autism spectrum: the role of development. J Am Acad Child Adolesc Psychiatry 48(5):471–473
23. Jones W, Carr K, Klin A (2008) Absence of preferential looking to the eyes of approaching adults predicts level of social disability in 2-year-old toddlers with autism spectrum disorder. Arch Gen Psychiatry 65(8):946–954
24. Gardner A (2010) New hope for early detection of autism. US News: Health Day. May 19, 2010
25. Damasio H, Damasio AR (1989) Lesion analysis in neuropsychology. New York, Oxford
26. Frey R, Woods DL, Knight RT, Scabini D (1987) Defining functional cortical areas with "averaged" CT scans. Soc Neurosci Abstr 13:1266–1267
27. Rorden C, Brett M (2000) Stereotaxic display of brain lesions. Behav Neurol 12(4):191–200
28. Brett M, Leff AP, Rorden C, Ashburner J (2001) Spatial normalization of brain images with focal lesions using cost function masking. Neuroimage 14(2):486–500
29. Fang Q, Boas DA (2009) Tetrahedral mesh generation from volumetric binary and gray-scale images. In: Proceedings of IEEE international symposium on biomedical imaging 2009, pp 1142–1145
30. Fang Q, Carp SA, Selb J, Moore R, Kopans DB, Miller EL, Brooks DH, Boas DA (2008) A multi-modality image reconstruction platform for diffuse optical tomography, Biomedical optics 2008, BIOMED poster session II (BMD), March 2008.
31. Zhang Y, Hamza A (2006) Vertex-based anisotropic smoothing of 3D mesh data, In: IEEE CCECE, pp 202–205
32. Cignoni P, Gobbetti E, Pintus R, Scopigno R (2008) Color enhancement for rapid prototyping. The 9th international symposium on vast international symposium on virtual reality, archaeology and cultural heritage, Eurographics, pp 9–16
33. Pitzalis D, Cignoni P, Menu M, Aitken G (2008) 3D enhanced model from multiple data sources for the analysis of the Cylinder seal of Ibni-Sharrum, The 9th international symposium on VAST international symposium on virtual reality, archaeology and cultural heritage, Eurographics, pp 79–84
34. Fornberg B (1998) A practical guide to pseudospectral methods. Cambridge University Press, Cambridge, UK

35. Chung MK, Shen L, Dalton KM, Evans AC, Davidson RJ (2007) Weighted Fourier representation and its application to quantifying the amount of gray matter. IEEE Trans Med Imaging 26:566–581
36. Courant R, Hilbert D (1953) Methods of mathematical physics, II. Interscience, New York, English edition
37. Chung MK, Dalton KM, Shen LL, Evans AC, Davidson RJ (2007) Weighted Fourier series representation and its application to quantifying the amount of gray matter. IEEE Trans Med Imaging 26:566–581

Biography

Matthew Nitzken is currently a student of the University of Louisville working on his Ph.D. studies. He holds a B.Eng. and M.Eng. degree in bioengineering from the University of Louisville, Louisville, KY. He has worked on shape analysis and medical imaging studies in his senior and graduate years of the program and plans to pursue this path in his future studies.

Ayman El-Baz received the B.Sc. and M.S. degrees in electrical engineering from Mansoura University, Egypt, in 1997 and 2000, respectively and the Ph.D. degree in electrical engineering from University of Louisville, Louisville, KY. He joined the Bioengineering Department, University of Louisville, in August 2006. His current research is focused on developing new computer assisted diagnosis systems for different diseases and brain disorders.

This figure will be printed in b/w

Manuel F. Casanova received his M.D. from the University of Puerto Rico in 1979. He received specialty training in neurology, neuropathology, and psychiatry. In 2003 he came to the University of Louisville where he is the Vice Chair for Research, Department of Psychiatry. His main focus of research is neurodevelopmental conditions, primarily autism.

Fahmi Khalifa received his B.Sc. and M.S. degrees in electrical engineering from Mansoura University, Mansoura, Egypt, in 2003 and 2007, respectively. In May 2009 he joined the BioImaging Laboratory at University of Louisville, Louisville, KY, USA, as a research assistance. His current research is focused on simultaneous image segmentation and registration with main focus on Automatic Diagnosis of Lung Cancer using Contrast Enhancement Computed Tomography Images.

Guela Sokhadze is a Psychology Major, and an undergraduate student of the University of Louisville. As well as working part time at BioImaging Laboratory, he assists at the Cognitive Neuroscience Lab in the Health Sciences Center. He is currently involved in multiple Neuroimaging studies of ADHD and Autism.

Author Queries

Chapter No.: 7

Query Refs.	Details Required	Author's response
AU1	Please check if the name 'Paolo Cignoli' can be replaced with 'Paolo Cignoni' in the sentence 'The mesh was loaded into the freely available software.....'.	
AU2	The terms 'theta and phi' have been replaced with 'θ and φ' throughout the document. Please check.	